Network Simulation of Steady-State Two-Phase Flow in Consolidated Porous Media

George N. Constantinides and Alkiviades C. Payatakes
Dept. of Chemical Engineering, University of Patras
Institute of Chemical Engineering and High Temperature Chemical Processes, GR 265 00 Patras, Greece

A computer-aided simulator of steady-state two-phase flow in consolidated porous media is developed. The porous medium is modeled as a 3-D pore network of suitably shaped and randomly sized unit cells of the constricted-tube type. The problem of two-phase flow is solved using the network approach. The wetting phase saturation, the viscosity ratio, the capillary number, and the probability of coalescence between two colliding ganglia are changed systematically, whereas the geometrical and topological characteristics of the porous medium and wettability (dynamic contact angles) are kept constant. In the range of the parameter values investigated, the flow behavior observed is ganglion population dynamics (intrinsically unsteady, but giving a time-averaged steady state). The mean ganglion size and fraction of the nonwetting phase in the form of stranded ganglia are studied as functions of the main dimensionless parameters. Fractional flows and relative permeabilities are determined and correlated with flow phenomena at pore level. Effects of the wetting phase saturation, the viscosity ratio, the capillary number, and the coalescence factor on relative permeabilities are examined.

Introduction

Multiphase flow in porous media is a complex process encountered in many fields of practical engineering interest, such as oil recovery from reservoir rocks, aquifer pollution by liquid wastes and soil reconstitution, and agricultural irrigation. Immiscible two-phase flow has many modes: steady state, imbibition, drainage, cocurrent, countercurrent, and so on. Here we are concerned with cocurrent steady-state flow. For the sake of brevity we will use the term oil to denote the nonwetting fluid, and water to denote the wetting fluid, with understanding that the two fluids can be other than oil and water. In particular, we are interested in the theoretical investigation of the flow regime of "steady-state" ganglion dynamics, which has been identified recently as one of the main flow regimes of steady-state cocurrent two-phase flow.

Recent experimental observations of steady-state flow of water and oil through planar and nonplanar chamber-and-throat pore networks etched in glass (Avraam et al., 1994; Avraam and Payatakes, 1995) have shown that over broad ranges of the values of the main dimensionless parameters (capillary number, viscosity ratio, water saturation) the oil is disconnected in the form of ganglia. Part of the oil in the pore network is stationary in the form of stranded ganglia, whereas the flowing part of the oil moves in the form of multisized ganglia. Moving ganglia that collide with others, which are either stranded or moving, and coalesce (or fail to coalesce) with them; moving ganglia frequently break into smaller ones, some of which become stranded, and so on. Stranded ganglia become remobilized if they coalesce with moving ones. Another important observation is that, often when a ganglion approaches a stranded one, it changes the local pressure field and may mobilize the stranded ganglion without actually colliding with it. The moving ganglia do not always follow the same paths, but sample large areas of the network, even though certain areas are visited more frequently than others. Ganglion motion and interactions result in an overall dynamic equilibrium giving a time-averaged steady state. Such a flow pattern is highly sensitive to the capillary number, the viscosity ratio, the saturation, the contact angle, the coalescence factor, and the geometry and topology of the pore network, and can be described as "*steady-state*" *ganglion dynamics*. Throughout the text, we use the term "steady state" in quotation marks to emphasize that what appears as steady-

state macroscopically is a process at dynamic equilibrium microscopically. The aforementioned experimental observations elucidate the flow mechanisms at pore level during "steady-state" two-phase flow experiments and show that moving disconnected oil is solely responsible for the oil flow rate in the flow regime under consideration. These observations disprove the common assumption that disconnected portions of oil do not move at all (for example, review by Honarpour and Mahmood, 1988; discussion in Avraam et al., 1994; Avraam and Payatakes, 1995).

Experimental studies have shown that relative permeabilities are strong functions not only of the saturation, but of the capillary number (Sanberg et al., 1958; Lefebvre du Prey, 1973; Amaefule and Handy, 1984; Fulcher et al., 1985; Avraam et al., 1994; Avraam and Payatakes, 1995), the viscosity ratio (Lefebvre du Prey, 1973; Fulcher et al., 1985; Avraam and Payatakes, 1995; although earlier experimental studies by Geffen et al., 1951 and Sanberg et al., 1958, had concluded that the effect of the viscosity ratio on the relative permeabilities was negligible), the contact angle (Geffen et al., 1951; Owens and Archer, 1971; McCaffey and Benion, 1974), the geometrical and topological characteristics of the porous medium (Lefebvre du Prey, 1973), and even the history of the experiment (wetting saturation increasing or decreasing). Here, we will demonstrate that relative permeabilities also depend on the coalescence factor, Co, which is the effective probability of coalescence given a collision between two ganglia in the porous medium (Constantinides and Payatakes, 1991). Since relative permeability values are strongly correlated with the flow regime, in other words, the morphology of the two phases (Payatakes and Dias, 1984; Sahimi, 1993; Avraam et al., 1994; Avraam and Payatakes, 1995) and for typical values of the dimensionless parameters, the oil exists in the form of ganglia, understanding ganglion dynamics is essential in understanding how relative permeabilities depend on the system parameters.

Two different methods have been proposed for modeling two-phase flow in porous media, namely percolation (Ramakrishnam and Wasan, 1986; Kantzas and Chatzis, 1988a,b; Blunt and King, 1991, 1992; Bryant and Blunt, 1992; Goode and Ramakrishnam, 1993) and network microflow simulation (Koplik and Lasseter, 1982; Dias and Payatakes, 1986a,b; Constantinides and Payatakes, 1988, 1991; Tsakiroglou and Payatakes, 1990, 1991; Vizika et al., 1994). Percolation models fail to take into account migration of ganglia and their interactions (Payatakes and Dias, 1984; Lenormand et al., 1988; Sahimi, 1993). The pore-network microflow simulator proposed here is an extension and generalization of the simulators of Dias and Payatakes (1986a,b) and Constantinides and Payatakes (1988, 1991), and is applicable to the modeling of ganglion dynamics and the prediction of "steady-state" relative permeabilities.

In this study the water saturation, S_w, the capillary number, Ca, the viscosity ratio, κ, and the probability of coalescence of two colliding ganglia, Co (we set $Co = C_{11}$) are changed systematically, whereas the porous medium model and dynamic contact angles, θ_a^0 and θ_r^0, are kept constant. For the ranges of the system parameter values investigated the oil remains disconnected. Under "steady-state" conditions, the reduced mean ganglion volume, $\langle v^* \rangle$, and the fraction of oil in the form of stranded ganglia, s, depend strongly on the values of the aforementioned parameters. The calculated "steady-state" relative permeabilities, k_{rw} and k_{ro}, depend on S_w, Ca, κ, and C_{11}. Fractional flow curves are calculated as well, and their dependence on the system parameters is examined. The validity of the simulator was examined in a case study, by comparing the theoretical predictions with experimental results of Avraam and Payatakes (1995). The agreement is very good.

Model Formulation

Construction of the porous medium model

The porous medium model used by the simulator is a three-dimensional network of unit cells of the constricted-tube type, suitable for consolidated porous media and has been described elsewhere (Constantinides and Payatakes, 1989). Here, we give just a brief description for the sake of completeness.

The skeleton of the network is a randomized lattice obtained as follows. We begin with a regular cubic skeleton, having length of periodicity l, coordination number, $\sigma = 6$, and M_x, M_y, and M_z nodes in the x, y, and z directions, respectively. Then each node is perturbed by being moved to a random position within an imaginary sphere centered at the original position of the node and having a preselected radius (equal to $0.2l$ for this study). The centers of the chambers coincide with nodes and the axes of the throats with the branches of the network. Here, we use chamber and throat diameter distributions based on experimental data for a Berea sandstone (Dullien and Dhawan, 1975). According to these data, the sizes of contiguous throats and chambers are positively correlated (large chambers are connected to large throats, and small chambers to small throats). The aforementioned correlation is realized in the pore network model by letting chambers influence the size of their neighboring throats, using the method of "voting" described by Constantinides and Payatakes (1989) and Tsakiroglou and Payatakes (1991). Numerical tests show that the best fit of the experimental bivariate pore size distribution is achieved when the value of the voting parameter, ξ, equals 1. The length of the periodicity, l, is selected so that the porosity of the pore network, ϵ, equals that of the prototype rock ($\epsilon = 0.22$). A two-layer pore network of size $30 \times 20 \times 2$ and $\xi = 1$ is shown in Figure 1a. To avoid a highly complicated figure we depict the chambers as spheres and the throats as cylinders. Solid volumes represent the upper layer of the network and dashed lines the lower one. In the drawing, the node-to-node distance increases by 50% for better clarity.

The pore network is divided into three zones: the inlet, the intermediate, and the outlet zone (Figure 1a). The inlet zone is geometrically the same with the outlet zone. The reason for using this zone arrangement is explained below. For this article, each zone has $10 \times 20 \times 5$ nodes, that is, the pore network has $30 \times 20 \times 5$ nodes. The two-layer version of this pore network is shown in Figure 1a.

To achieve a simple mathematical treatment of the flow problem, the porous medium model is considered as a network of unit cells of the constricted-tube type, as shown in Figure 1b. Each unit cell consists of a tubular part that represents a throat and two sinusoidal segments that are parts of adjacent chambers. Unit cells of this type are suitable in

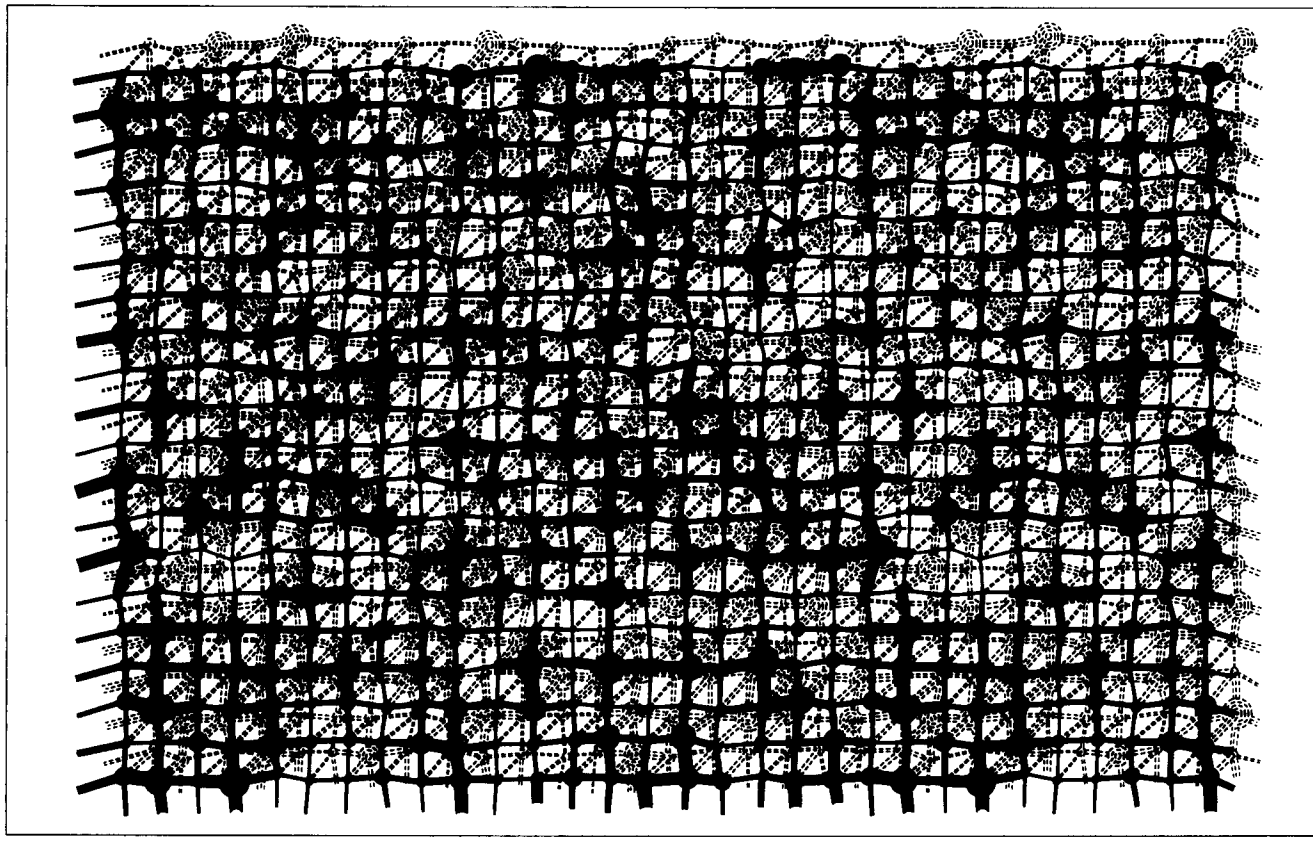

Figure 1a. Representative randomized two-layer pore network.

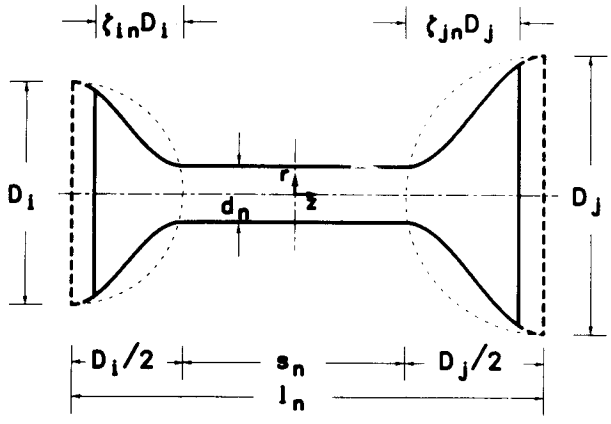

Figure 1b. Representative unit cell.

modeling consolidated porous media (such as sandstones). The theoretical absolute permeability, k, calculated by averaging calculated permeabilities of 20 finite networks of size $30\times20\times5$, is $k=1.05\pm0.08$ darcy ($=1.04\pm0.08\ \mu m^2$).

Simulation of "steady-state" ganglion dynamics

Under creeping flow conditions, the two-phase flow through the pore network is solved with standard network analysis, recognizing the analogy between pressure difference and potential difference, hydraulic conductance and electrical conductance, flow rate and current, and capillary pressure and electromotive force (Dias and Payatakes, 1986a,b; Constantinides and Payatakes, 1991; Vizika et al., 1994).

Initially the network is filled with water. Ganglia of preselected volumes and random shapes are placed in the network, until the saturation of oil takes a preselected value, S_o. The macroscopic pressure gradient, $-\nabla P$, applied along the pore network is determined by trial and error, so that the desirable value of the "steady-state" capillary number Ca is achieved. The capillary number is defined as $Ca=U_w\mu_w/\gamma$, where U_w is the superficial velocity of water at "steady-state" conditions, μ_w is the viscosity of water, and γ is the interfacial tension. The pressure drop along the network is given by

$$P_I - P_O = (-\nabla P)l(M_x+1), \tag{1}$$

where P_I is the pressure of a reservoir that is connected with all $M_y\times M_z$ unit cells at the inlet of the network, and P_O is the pressure of a sink which is connected with all $M_y\times M_z$ unit cells at the outlet of the network (for simplicity, $P_O=0$). The boundary conditions on the sides parallel to the macroscopic flow are assumed to be periodical, so that the network considered represents a strip of infinite dimensions in the y and z directions.

Each unit cell is regarded as a resistor, and its resistance is set equal to the sum of the hydraulic resistances of the cylindrical and the two sinusoidal segments of the cell, whereas the capillary pressure drop across a meniscus is calculated using a Washburn-type approximation. (Details of the calcu-

lation of the hydraulic resistances and the pressure drops across interfaces are given by Dias and Payatakes, 1986a, and Vizika et al., 1994.)

The solution of the two-phase flow problem is obtained in a stepwise manner, assuming pseudosteady state at each step. The systems of linear equations describing the pseudosteady flow at each step is solved with the Cholesky decomposition procedure, suitably modified to take into account the high sparseness of the matrix, and the instantaneous values of the pressure at the nodes of the network are calculated. These pressure values are, in turn, used to calculate the instantaneous flow rates through the unit cells and the corresponding velocities of the menisci. Assuming these velocities to remain constant over an appropriately small time interval (Dias and Payatakes, 1986a), new positions for the menisci at the end of the time step can be calculated, and the process is repeated.

When a unit cell becomes filled with oil or water, the approach that is adopted in order to decide what configuration to assign to the new interface is an extension of that described in Dias and Payatakes (1986a), taking into account the three-dimensional topology of the pore network. The procedure followed for the disconnection of oil is basically the same with that proposed by Dias and Payatakes (1986a). Note here that disconnection of oil due to pinch-off takes place only inside chambers (Li and Wardlaw, 1986), because we consider intermediate contact angle systems ($\theta \approx 40°$).

When the viscous forces that act on a ganglion are balanced by the capillary ones, the ganglion becomes stranded. In the Dias and Payatakes simulator, the pressure drop along the ganglion, which is needed to apply the stranding criterion, is estimated based on the macroscopic pressure gradient, using the smooth field approximation. In our simulator the exact pressure drop calculated by the network model is used, and so the stranding criterion is applied more precisely. For computational reasons, conductances of the unit cells occupied by a stranded ganglion are set equal to nil, and the ganglion is "frozen" in place. In applying the stranding criterion the capillary pressure difference is calculated using the upper bound of the drainage curvature for downstream menisci and the lower bound of the imbibition curvature for upstream menisci (Dias and Payatakes, 1986a). Hence, the capillary pressure difference is slightly overestimated and the ganglion becomes stranded for slightly higher pressure difference than the exact one. A check for the possibility of remobilization of each ganglion is done each time the pressure field values are updated, by comparing the viscous forces causing mobilization and the capillary ones opposed to the motion. This is basically the criterion for ganglion mobilization developed by Ng and Payatakes (1980) (see also, Payatakes, 1982; Mason, 1983; Payatakes and Dias, 1984) used with the exact pressure values calculated with the network approach. If a ganglion can be mobilized, it is set free by becoming "unfrozen" and the conductances of the corresponding unit cells are set to their proper values.

As ganglia are being displaced by water, two portions of two individual ganglia may meet each other in the same pore. If the water that separates the two oil fingers can escape out of the pore, it gradually takes the form of a thin film and may eventually collapse under the influence of the London–van der Waals force. The rate of film drainage is affected by several obvious factors (local pore geometry, the positions of the two menisci, the viscosities of the two fluids, the local pressure field in each phase, etc.), and furthermore by the surface viscosities, the surface elasticities, and the concentration of surfactant(s) on the interfaces (Ivanov and Dimitrov, 1988). Coalescence will be prevented if one or both oil bodies move away due to the bulk motion of the ganglia to which they belong. A model incorporating the flow of the water film, interactions of the two approaching oil bodies, and the bulk motion of the ganglia has been developed by Constantinides and Payatakes (1991). In that work, as in this article, both oil and water were considered to be pure liquids. The presence of electrolyte(s) and/or surfactant(s) would cause Marangoni effects, electrostatic interactions between interfaces, change of the flow properties of each interface, and reduction of the interface mobility, which would lower the rate of the film drainage and consequently the rate of coalescence. The aforementioned model was used to evaluate the probability of coalescence between two colliding moving ganglia, C_{11}. It was shown that C_{11} depends strongly on the hydraulic conductance of the pore wall microroughness, the shapes and volumes of the colliding ganglia, the local geometry and topology of the porous medium, the dynamic contact angles, and weakly on the viscosity ratio, κ, and the capillary number, Ca. According to the present simulator, the two oil bodies meeting each other in the same unit cell coalesce with a fixed probability C_{11} (equal to the coalescence factor, Co, which is defined as the effective probability of coalescence given a collision in systems flowing through ganglion dynamics). The water trapped between the two menisci can escape toward nearby areas of the network that are occupied by water and have a smaller pressure than the pressure of the trapped water. This leakage can occur through narrow passages provided by the roughness features and crevices of the pore walls.

As ganglia migrate downstream, the inlet zone of the network would be evacuated from ganglia progressively were it not for the fact that replicas of ganglia that leave the intermediate zone and move to the outlet zone are being introduced at the corresponding sites of the inlet zone. In this way, a kind of periodicity in the direction of flow and a nearly constant oil saturation are achieved. Here, we have to emphasize that although the inlet and the outlet zones are geometrically the same, the flow fields in these zones are different. This happens because the entrance unit cells of the inlet zone are connected with a reservoir of constant pressure, P_I, whereas the corresponding unit cells of the outlet zone are connected with the intermediate zone, where the pressure varies with time and from node to node. Also, the exit unit cells of the outlet zone are connected with a sink of constant pressure, P_O, whereas the corresponding unit cells of the inlet zone are connected with the intermediate zone.

In this simulator gravity effects have been neglected, since for typical values of the parameters (difference of densities of the two fluids, $\Delta\rho = 200$ kg/m^3, mean throat diameter, $\langle d \rangle = 17.72$ μm, interfacial tension, $\gamma = 25$ mN/m) the Bond number is $Bo = \Delta\rho g \langle d \rangle^2 / 4\gamma = 6 \times 10^{-6}$.

Calculation of "steady-state" relative permeabilities

The calculation of the instantaneous values of the relative permeabilities to both fluids is done in the following way. A

region of the pore network at the boundary of the inlet with the intermediate zone is selected. This region has dimensions of three chambers in the direction of flow (x-direction), that is, one chamber in the inlet zone and two chambers in the intermediate zone, 15 chambers in the y-direction, and three chambers in the z-direction. At the end of a time step, some of these chambers are occupied by water and the rest by oil. During this time step, the values of the pressure at the centers of chambers (nodes) are known (see above). The mean pressure of water in this region is calculated by averaging the instantaneous pressure values at the chambers occupied by water, whereas the mean pressure of oil by averaging the instantaneous pressure values at the chambers occupied by oil. Another region including the same number of chambers is selected at the boundary of the intermediate with the outlet zone. The center of the second region is $L = 10l$ distant from the center of the first one. The mean pressures of both phases in the second region are calculated as in the first one. Hence, the instantaneous pressure drops of water and oil along the network, ΔP_w and ΔP_o, respectively, can be calculated. The calculation of the instantaneous flow rates of the water and oil, q_w and q_o, is done as follows. The area of the pore network over which the pressure drops are calculated is divided into sections. Each section includes one chamber (and the two half-throats connected to it) in the x-direction and all the chambers in the y- and z-directions. At the end of each time step the flow rates through the unit cells (and thus through the throats) are known. Hence, the total instantaneous flow rates of both fluids flowing through each section can be calculated by totaling the respective flow rates through the appropriate throats. The mean instantaneous flow rates of the two fluids are calculated by averaging the respective values of flow rates of the sections. Given the instantaneous values of the pressure drops along the network and the flow rates of the two fluids, the *instantaneous* relative permeabilities, k'_{rw} and k'_{ro}, respectively, are calculated using the expressions

$$\frac{q_w}{A} = -k'_{rw}\frac{k}{\mu_w}\frac{\Delta P_w}{L} \tag{2}$$

$$\frac{q_o}{A} = -k'_{ro}\frac{k}{\mu_o}\frac{\Delta P_o}{L}, \tag{3}$$

where A is the cross-sectional area of the pore network.

The values of "steady-state" relative permeabilities, k_{rw} and k_{ro}, are obtained as the time-averaged values of the instantaneous relative permeabilities over a sufficiently long time interval (see below) during which the fluids flow under "steady-state" conditions. Simulations showed that the "steady-state" relative permeabilities, k_{rw} and k_{ro}, are independent of the length and the exact location of the area of pore network along which the pressure drops are calculated, so long as this area is away from the entrance and the exit of the pore network.

Results and Discussion

Sample stochastic simulations of "steady-state" ganglion dynamics

The simulation of "steady-state" ganglion dynamics begins by placing ganglia of constant initial volume and random shapes at random sites of the network, until oil saturation becomes equal to a preselected value, S_o. For the simulations of this work, the reduced volume of each ganglion initially placed in the network is $v^*_{in} = 3$, unless otherwise stated. (The reduced ganglion volume, v^*, is the ratio of the actual volume of the ganglion to the average volume of a Conceptual Elemental Void Space, that is, a chamber and its adjacent σ half-throats.) Then, a macroscopic pressure drop is applied and the ganglia are let to move. Some of the ganglia become trapped where they were placed, while the rest begin to migrate downstream. The modes of ganglion displacement observed are quasi static and dynamic (Payatakes, 1982; Dias and Payatakes, 1986b; Hinkley et al., 1987). We find that the two modes operate simultaneously due to the high degree of randomness of the pore network. Moving ganglia fission into daughter ganglia, the smaller ones of which usually become stranded where they are formed, or after a few steps. The breakup mechanisms considered in the simulator are pinch-off (rupture of oil threads inside chambers) and dynamic breakup (Payatakes and Dias, 1984). Breakup by pinch-off occurs for all values of the dimensionless parameters investigated. As Ca and/or S_o increase, and/or κ decreases, dynamic breakup intensifies. If a moving ganglion comes in the vicinity of a stranded one, then it changes the local pressure field, and the stranded ganglion may become remobilized. If remobilization is not possible under the circumstances, then the moving ganglion bypasses the stranded one. Both remobilization and bypassing are enhanced by relatively high Ca and/or low κ values. Moving ganglia collide and coalesce with a fixed probability C_{11} with other moving ones and form larger ganglia. The number of collisions per time step depends on the value of S_o and the mean ganglion size (see below). Combination of the preceding phenomena results in an overall dynamic equilibrium, which is denoted as *"steady-state" ganglion dynamics*. A snapshot of the distribution of oil at $t^* = 300$ and for $\kappa = 0.67$, $Ca = 10^{-4}$, $C_{11} = 0.15$, $S_w = 50\%$ PV, $\theta_a^0 = 45°$, and $\theta_r^0 = 35°$ is shown in Figure 2. For clarity, the two-layer pore network of size $30 \times 20 \times 2$ and $\xi = 1$ shown in Figure 1a is used for this simulation (note that all the other simulations presented in this work were performed in a network of size $30 \times 20 \times 5$), and only the pores occupied by oil have been plotted. Figure 3 shows a snapshot of oil distribution from a similar simulation, using $\kappa = 3.35$ (value of κ five times larger than that of Figure 2), whereas values of the other parameters and the pore network are kept the same.

We define as "steady state" that in which the time-averaged values of *all* the main variables (relative permeabilities, number of ganglia, reduced mean ganglion volume, fraction of oil in the form of stranded ganglia, fractional flows, etc.) remain constant. Usually, all the main variables reach "steady-state" at the same time. The time needed by a ganglion population to achieve "steady-state" conditions depends on the system parameters. For all the simulations performed this reduced time, t^*, is less than 50. The reduced time, t^*, is defined as the real time elapsed divided by the characteristic time $t_{ch} = l\epsilon/U_w$.

Figure 4 shows the time dependence of the instantaneous relative permeability to oil, k'_{ro} ($\kappa = 3.35$, $Ca = 10^{-4}$, $C_{11} = 0.15$, $S_w = 50\%$ PV, $\theta_a^0 = 45°$, and $\theta_r^0 = 35°$) and the effect of the initial conditions on k'_{ro} (here, the period of transient flow lasts approximately $t^* = 30$). Three different initial con-

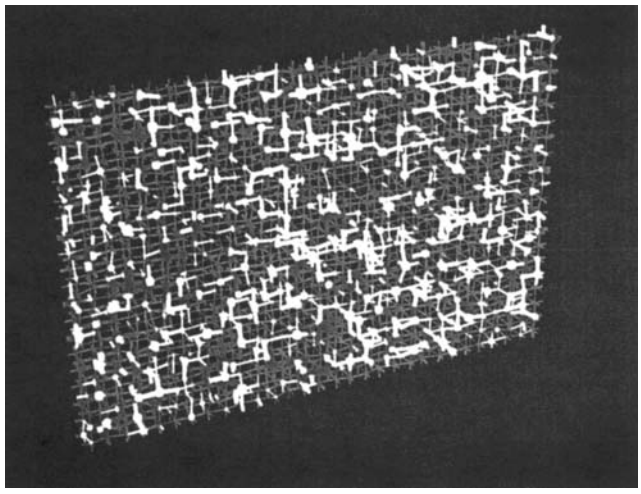

Figure 2. Distribution of oil in the pore network at $t^* = 300$ and for $\kappa = 0.67$, $Ca = 10^{-4}$, $C_{11} = 0.15$, $S_w = 50\%$ PV, $\theta_a^0 = 45°$, and $\theta_r^0 = 35°$.

Oil is shown white and water is shown gray. The macroscopic flow is from left to right (see text).

ditions are considered. In the first case, the reduced volume of each ganglion, initially placed in the pore network, is $v_{in}^* = 1$, whereas in the second case it is $v_{in}^* = 3$, and in the third $v_{in}^* = 9$. As Figure 4 shows, the "steady-state" relative permeability of oil remains the same in all three cases. We performed many simulations changing the initial conditions (value of v_{in}^*, initial shapes of the ganglia, and sites where the ganglia were initially placed). In all cases the "steady-state" values of the variables investigated were virtually independent on the initial conditions.

In addition, Figure 4 shows that under "steady-state" conditions the instantaneous relative permeability to oil, k'_{ro}, oscillates aperiodically around a mean value for all cases examined. The same behavior is also observed for all the other variables, namely k'_{rw}, ΔP_w, ΔP_O, q_w, q_o, the instantaneous number of ganglia, N_g, and so forth. Such diagrams indicate that the dynamic system under consideration behaves chaotically, and that each main variable has a powerful attractor. A study of the dynamic behavior of these systems is the subject of a forthcoming publication.

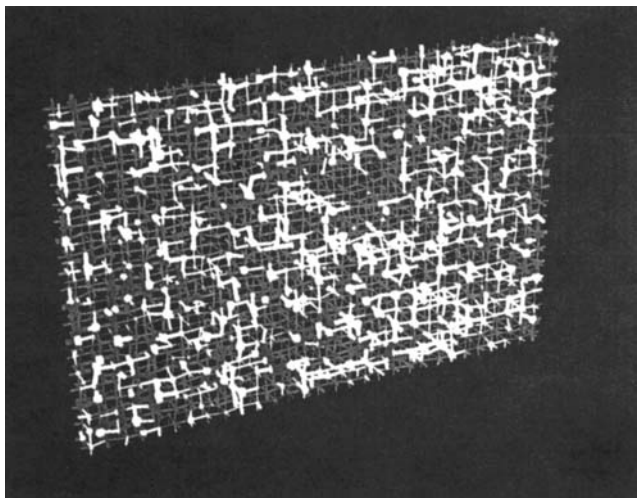

Figure 3. Distribution of oil in the pore network at $t^* = 300$ and for $\kappa = 3.35$, $Ca = 10^{-4}$, $C_{11} = 0.15$, $S_w = 50\%$ PV, $\theta_a^0 = 45°$, and $\theta_r^0 = 35°$.

Oil is shown white and water is shown gray. The macroscopic flow is from left to right (see text).

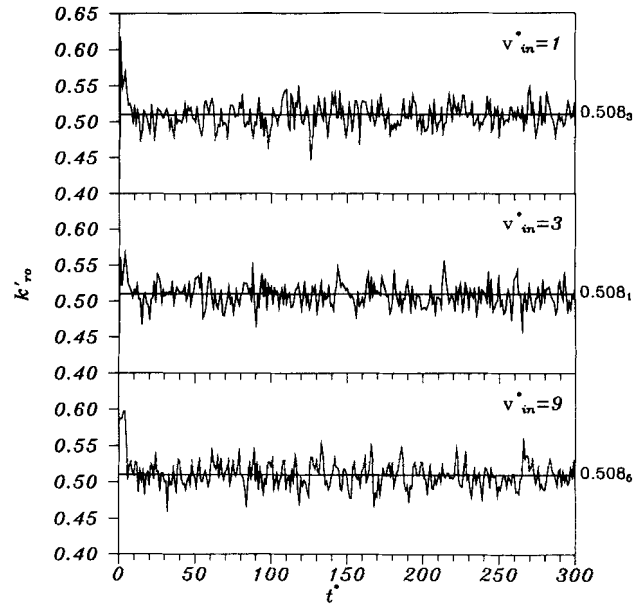

Figure 4. Time series of the instantaneous relative permeability to oil, k'_{ro} ($\kappa = 3.35$, $Ca = 10^{-4}$, $C_{11} = 0.15$, $S_w = 50\%$ PV, $\theta_a^0 = 45°$, and $\theta_r^0 = 35°$).

For three different initial conditions: the reduced volume of the ganglia initially placed in the pore network is $v_{in}^* = 1$, 3, and 9

All simulations reported in this work were terminated at $t^* = 300$. This means that the "steady-state" values of the main variables (k_{rw}, k_{ro}^*, $\langle v^* \rangle$, s, f_w, etc.) are calculated by averaging over a period $\Delta t^* \geq 250$. Under such conditions, the error bars (for confidence level 95%) of the "steady-state" values of all the variables investigated are too small to be shown. All simulator runs were performed using a HP Apollo 9000 workstation, Model 710. The average CPU time required for each simulation was approximately 5 days or more.

Flow mechanisms at pore level

Our simulations show that the path followed by a moving ganglion is determined by the outcome of competition of two factors. The first factor is the tendency of the ganglion to follow the direction of the macroscopic flow, and the second one is the tendency to move through large pores because in those the capillary resistance to the flow is relatively small. The second factor becomes even more important for high κ and low Ca values, because then large pores also offer the advantage of relatively small viscous dissipation. This effect is shown qualitatively in Figures 2 and 3. Although for both cases most of the ganglia undergo dynamic (as opposed to quasi-static) displacement, the tendency of the ganglia for $\kappa = 0.67$ to become long and more closely aligned with the di-

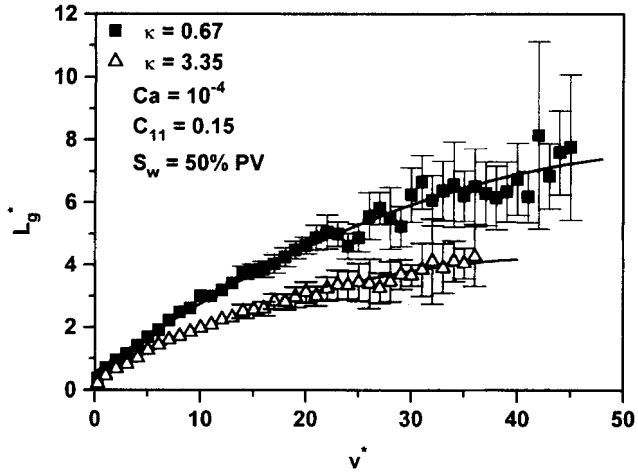

Figure 5. Mean reduced maximum length of the ganglia.

Projected in the direction of the macroscopic flow, L_g^*, as a function of their reduced ganglion volume, v^*, for $\kappa = 0.67$ and 3.35 and $Ca = 10^{-4}$, $C_{11} = 0.15$, $S_w = 50\%$ PV, $\theta_a^0 = 45°$, and $\theta_r^0 = 35°$.

rection of macroscopic flow is much higher than that for $\kappa = 3.35$. This observation is shown quantitatively in Figure 5. Ganglia have been classified according to their volumes. Each class contains all the ganglia with reduced volumes v^* in the interval $(v^* - 0.5, v^* + 0.5)$. For each class the mean value of the reduced maximum lengths (actual lengths divided by the length of periodicity, l) of the ganglia, projected in the direction of the macroscopic flow, L_g^*, are shown vs. their reduced ganglion volumes, v^*, for the aforementioned two cases ($\kappa = 0.67$ and 3.35; $Ca = 10^{-4}$, $C_{11} = 0.15$, $S_w = 50\%$ PV, $\theta_a^0 = 45°$, and $\theta_r^0 = 35°$). Error bars (confidence level 95%) are very small to show for $v^* \leq 13$. The two simulations were performed using the pore network size $30 \times 20 \times 5$.

In order to understand this behavior, we calculate the reduced volume of oil, V_{oil}^*, which flows through each of the unit cells residing on branches that used to be parallel to the macroscopic flow direction before the randomization of the network skeleton, for a specific time interval ($\Delta t^* = 250$) during the period of "steady-state" flow. (The number of the unit cells under consideration is 3,100 for the pore network we use.) Then, we correlate V_{oil}^* with the reduced specific hydraulic conductivity of the cell, $\hat{g}^*$. The reduced volume of oil, V_{oil}^*, which flows through each unit cell under consideration, is the ratio of the actual volume of oil to the average volume of a Conceptual Elemental Void Space (that is, a chamber and its adjacent σ half-throats), whereas the reduced specific hydraulic conductivity of a unit cell, $\hat{g}^*$, is the ratio of the actual specific hydraulic conductivity, $\hat{g}$, to the characteristic specific hydraulic conductivity, $\hat{g}_{ch}$. The specific hydraulic conductivity of the nth unit cell, $\hat{g}_n$, is defined as $\hat{g}_n = g_n \mu$, depends only on the geometrical characteristics of the unit cell, and has dimensions of volume. If the nth unit cell were to be replaced by a cylindrical capillary of diameter d_n and length l_n (Figure 1b), its specific hydraulic conductivity, $\hat{g}'_n$, would be $\hat{g}'_n = \mu q_n / \Delta P_n = (\pi/128)(d_n^4/l_n)$, where q_n is the flowrate through the capillary and ΔP_n the pressure drop along the capillary. The characteristic specific hydraulic conductivity, $\hat{g}_{ch}$, is defined as $\hat{g}_{ch} = \langle \hat{g}'_n \rangle = (\pi/128)\langle d_n^4/l_n \rangle$.

Figures 6a and 6b show the correlation of $\hat{g}^*$ and V_{oil}^* for $\kappa = 0.67$ and 3.35, respectively ($Ca = 10^{-4}$, $C_{11} = 0.15$, $S_w = 50\%$ PV, $\theta_a^0 = 45°$, $\theta_r^0 = 35°$). Correlation coefficients for these two cases are $R = 0.689$ for $\kappa = 0.67$ and $R = 0.797$ for $\kappa = 3.35$. As κ increases the oil prefers to flow through the unit cells with relatively large specific hydraulic conductivity. This phenomenon can have profound consequences on the flow regime, leading from "steady-state" ganglion dynamics to connected-oil pathway flow under certain conditions. If the network contains strings of large pores (which is the case when there is a significant positive correlation of the sizes of contiguous pores; Constantinides and Payatakes, 1989), if Ca is relatively high (say $Ca > \sim 10^{-5}$), and if the coalescence factor is large (say $Co \rightarrow 1$), the oil flow will be concentrated

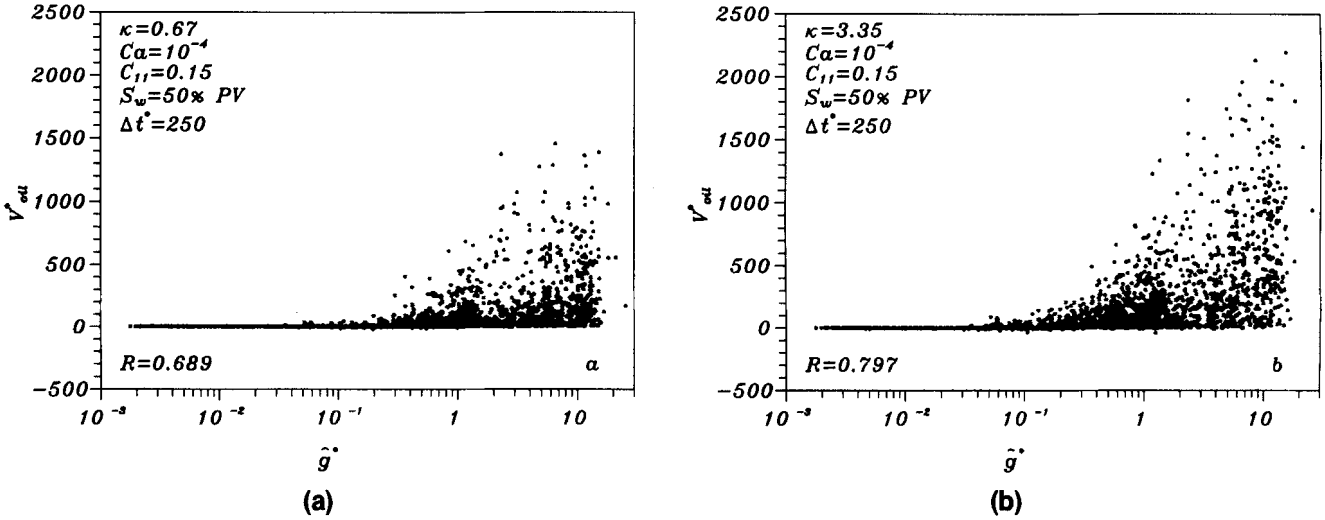

Figure 6. Correlation of the reduced specific conductivity of the unit cells, $\hat{g}^*$, and the reduced volume of oil, V_{oil}^*.

Oil was passed through each of the cells residing on branches, which used to be parallel to the macroscopic flow direction before network randomization, for a specific interval time ($\Delta t^* = 250$) and for: (a) $\kappa = 0.67$, $Ca = 10^{-4}$, $C_{11} = 0.15$, $S_w = 50\%$ PV, $\theta_a^0 = 45°$, and $\theta_r^0 = 35°$; (b) $\kappa = 3.35$, $Ca = 10^{-4}$, $C_{11} = 0.15$, $S_w = 50\%$ PV, $\theta_a^0 = 45°$, and $\theta_r^0 = 35°$.

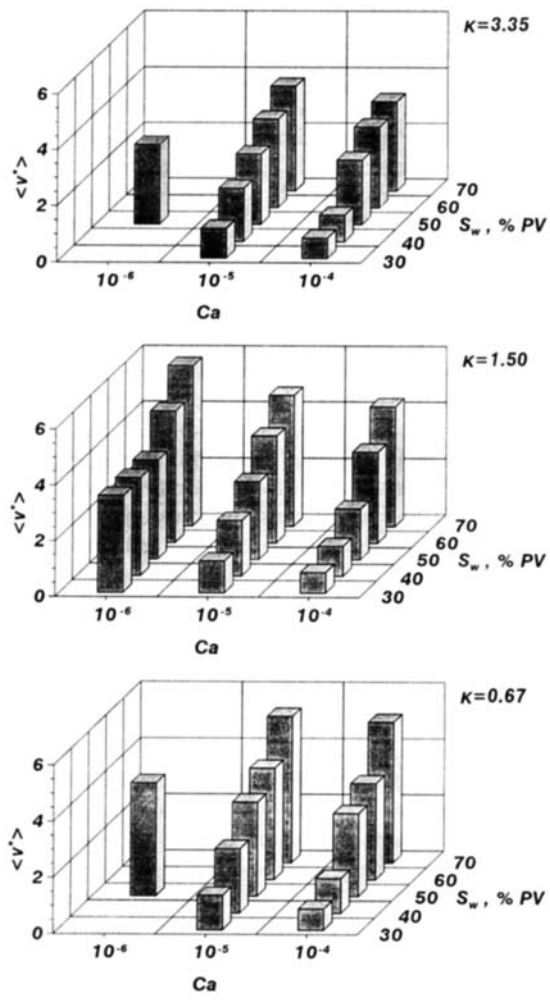

Figure 7. Map of the "steady-state" reduced mean ganglion volume, $\langle v^* \rangle$, as a function of the capillary number, Ca, the water saturation, S_w, and the viscosity ratio, κ.

For $C_{11} = 0.15$, $\theta_a^0 = 45°$, and $\theta r^0 = 35°$.

along pathways composed of large pores. This tendency would lead to high oil saturation along these pathways and, consequently, the formation of connected oil pathways through frequent collisions and prompt coalescence. The appearance of this flow regime would be enhanced further by high S_o and large κ values. This type of behavior has been reported by Avraam and Payatakes (1995). (The performance of the present simulator in the domain of connected-oil pathway flow is the subject of ongoing work.)

The correlation coefficients of $\hat{g}^*$ and V_{oil}^* for $Ca = 10^{-4}$ and 10^{-5} ($\kappa = 1.50$, $Ca = 10^{-4}$, $C_{11} = 0.15$, $S_w = 50\%$ PV, $\theta_a^0 = 45°$ and $\theta_r^0 = 35°$) are $R = 0.738$ and $R = 0.757$, respectively. For $Ca = 10^{-5}$ most of the ganglia move in the quasi-static mode and they follow paths that reduce viscous dissipation, whereas for $Ca = 10^{-4}$ most of the ganglia are displaced under dynamic conditions and move through both large and small pores.

A significant factor in "steady-state" two phase flow is the size of the ganglia. The ganglion size distributions under "steady-state" conditions resemble log-normal distributions for all the values of the parameters investigated. A histogram showing the dependence of the "steady-state" reduced mean ganglion volume, $\langle v^* \rangle$, on the main dimensionless parameters (S_w, κ, Ca) for $C_{11} = 0.15$, $\theta_a^0 = 45°$, and $\theta_r^0 = 35°$ is given in Figure 7. The reduced mean ganglion volume, $\langle v^* \rangle$, decreases as Ca increases. This happens because as Ca increases (keeping the other parameters constant) the dynamic breakup intensifies. As mentioned earlier, as κ increases, ganglia tend to flow through large pores. Hence, for relatively high κ values, many long oil threads are formed and breakup by pinch-off is enhanced. Therefore, the reduced mean ganglion volume, $\langle v^* \rangle$, decreases as κ increases (keeping the parameters constant). As S_w decreases, the portion of the pore network through which water flows also decreases, and therefore both the "steady-state" interstitial water velocity and the local pressure gradient increase (for Ca = constant). Hence, dynamic breakup occurs more frequently as S_w decreases (keeping the other parameters constant) and thus $\langle v^* \rangle$ decreases. Besides, for relatively high water saturation values (say, $S_w = 70\%$ PV) the ganglion population is sparse. This means that interactions between ganglia (collisions followed by coalescence, remobilizations of stranded ganglia, etc.) occur less frequently. Therefore, if a large ganglion is stranded, it has a diminished probability of becoming remobilized. Consequently, $\langle v^* \rangle$ is relatively large for large S_w values. The results presented in the histogram of Figure 7 are in qualitative agreement with existing experimental data (Avraam et al., 1994; Avraam and Payatakes, 1995).

The fraction of oil that exists in the form of stranded ganglia, s, is plotted in Figure 8, as a function of S_w, κ, and Ca, and for $C_{11} = 0.15$, $\theta_a^0 = 45°$, and $\theta_r^0 = 35°$. This dependence can be explained based on the effects of the flow parameters on the reduced mean ganglion size at "steady state," $\langle v^* \rangle$, which were examined earlier. As Ca decreases (keeping the other parameters constant), the local pressure gradient also decreases and the amount of oil in the form of stranded ganglia, s, increases. A crucial variable involved in stranding is the maximum length of the ganglion, projected in the direction of macroscopic flow. Actually, the viscous force that is responsible for ganglion mobilization is proportional to this length and the local pressure gradient (Ng and Payatakes, 1980). For given flow conditions and physicochemical properties (interfacial tension, viscosities, dynamic contact angles), as this projected length decreases, the probability of stranding increases (Ng and Payatakes, 1980). The reduced mean ganglion volume, $\langle v^* \rangle$, as well as the mean ganglion length projected in the macroscopic flow direction decrease as κ increases (Figure 5). Hence, s increases as κ increases (keeping the other parameters constant). As S_w increases, the value of the macroscopic pressure gradient decreases and the interactions between ganglia become less frequent (see before). Therefore, as S_w increases (keeping the other parameters constant) more ganglia become stranded, and s increases.

Comparing Figures 7 and 8, it can be seen that for constant κ and Ca, as S_w decreases (S_o increases) both s and $\langle v^* \rangle$ decrease. At first sight this result seems strange, not to say, contradictory, since larger ganglia have a smaller probability of stranding, all other factors being equal. The explanation lies in the effect of S_w on the pressure gradient for constant Ca. As S_w decreases, the pressure gradient for constant

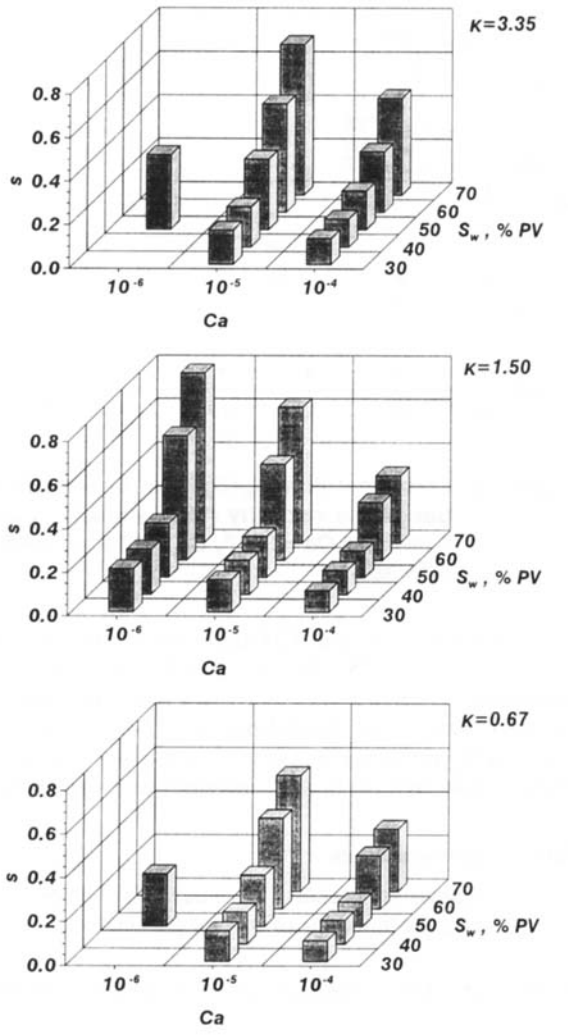

Figure 8. Map of the "steady-state" fraction of oil in the form of stranded ganglia, s, as a function of the capillary number, Ca, the water saturation, S_w, and the viscosity ratio, κ.

For $C_{11} = 0.15$, $\theta_a^0 = 45°$, and $\theta_r^0 = 35°$.

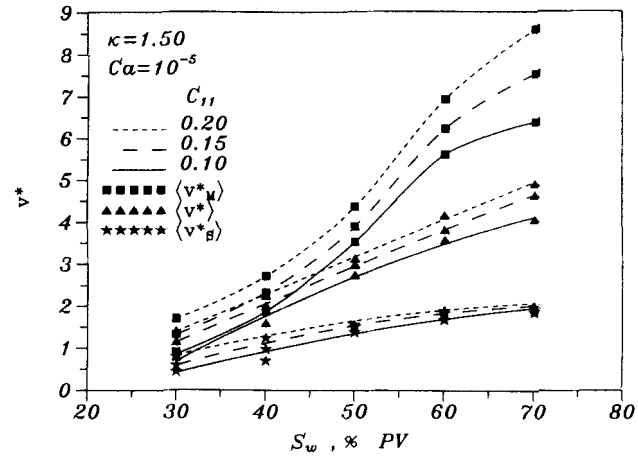

Figure 9. Dependence of the "steady-state" reduced mean ganglion volume, $\langle v^* \rangle$, reduced mean volume of the moving ganglia, $\langle v_M^* \rangle$, and reduced mean volume of the stranded ganglia, $\langle v_S^* \rangle$, on water saturation, S_w.

For three typical values of the probability of coalesence between two colliding ganglia ($C_{11} = 0.10$, 0.15, and 0.20) and $\kappa = 1.50$, $Ca = 10^{-5}$, $\theta_a^0 = 45°$, and $\theta_r^0 = 35°$.

Ca increases sharply because the relative permeability to water, k_{rw}, decreases sharply (see below), and this effect more than compensates for the decrease of the projected ganglion length. Thus, the critical projected ganglion length for stranding decreases as S_w decreases with constant Ca, and therefore s decreases *despite* the reduction of the average ganglion size. This effect was predicted in Ng and Payatakes (1980), where it was pointed out that in the case of ganglion populations the stranding coefficient should be calculated based on the value of Ca/k_{rw} rather than that of Ca alone.

The probability of coalescence between two colliding ganglia, C_{11}, plays a crucial role in ganglion dynamics. Under "steady-state" conditions, as C_{11} increases coalescence intensifies, and the reduced mean ganglion volume, $\langle v^* \rangle$, increases (Figure 9), if the rest of the parameters (S_w, Ca, κ, θ_a^0, θ_r^0, and the geometrical and topological characteristics of the porous medium) are kept constant. This means that the increase of C_{11} more than compensates for the increased rate of breakup. The reduced mean volume of the moving ganglia, $\langle v_M^* \rangle$, shows the same behavior (Figure 9): it is an increasing function of C_{11}, keeping the other parameters constant. The results of the increase of C_{11} are magnified for relatively high oil saturations, because in these cases collisions between ganglia occur more frequently. However, as S_w decreases, the pressure gradient increases sharply for a constant Ca value (see earlier), causing more frequent ganglion fissioning due to the intensified dynamic breakup. For this reason the increase of $\langle v^* \rangle$ and $\langle v_M^* \rangle$ as C_{11} increases is shown magnified only for high S_w values (Figure 9). The increase of the mean ganglion volume, as C_{11} increases, reduces the total number of ganglia for a given oil saturation value. Thus, as C_{11} increases, the oil ganglia become larger and fewer per unit volume. Under these conditions, remobilization of stranded ganglia due to transient changes of the local pressure field, caused by moving ganglia, is not frequent. This has two main consequences. First, the reduced mean volume of the stranded ganglia, $\langle v_S^* \rangle$, increases, as C_{11} increases (Figure 9), if the other parameters are kept constant. Note that, if the interactions between ganglia had been neglected, $\langle v_S^* \rangle$ would be independent of C_{11}, because the values of the parameters affecting ganglion entrapment remain constant. Second, the volume fraction of oil in the form of stranded ganglia, s, increases, as C_{11} increases (Figure 10). The observation that the value of s is high for high values of $\langle v^* \rangle$ for constant κ and Ca viscosity ratio is made here, as well. (See Figures 7 and 8 and the relevant earlier discussion.)

Fractional flows

The fractional flow of water is defined as $f_w = q_w/(q_w + q_o) = 1/(1 + r)$. In our simulator the flowrate ratio, $r = q_o/q_w$, is equal to the volume ratio, V_o/V_w, where V_o is the total volume of the ganglia being placed in the inlet zone during a length of time Δt^* of "steady-state" flow in order to keep S_o

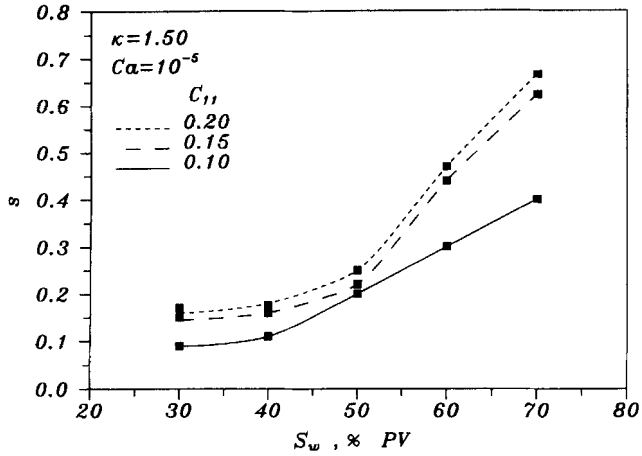

Figure 10. Dependence of the "steady-state" fraction of oil in the form of stranded ganglia, s, on water saturation, S_w.

For three typical values of the probability of coalescence between two colliding ganglia ($C_{11} = 0.10$, 0.15, and 0.20) and $\kappa = 1.50$, $Ca = 10^{-5}$, $\theta_a^0 = 45°$, and $\theta_r^0 = 35°$.

constant, and V_w is the total volume of water that enters into the pore network during the same length of time. Figure 11 shows the dependence of f_w on Ca and S_w for $\kappa = 1.50$, $C_{11} = 0.15$, $\theta_a^0 = 45°$, and $\theta_r^0 = 35°$. As Ca decreases and/or S_w increases, f_w increases, according to the familiar S-shape of most experimental curves. This result also agrees qualitatively with the experimental data of Avraam et al. (1994) and Avraam and Payatakes (1995). The values of the fractional flow of water, f_w, are related with the respective values of the fraction of oil in the form of stranded ganglia, s. For constant Ca, q_w also remains constant, and the volume of water that enters in the pore network for a given length of time, V_w, is fixed. For a given saturation, S_o (and thus S_w), the volume of the ganglia placed in the inlet zone, V_o (and thus the volume ratio V_o/V_w), decreases as s increases. Hence, f_w increases as s increases for the same Ca and S_o values. This behavior is shown in Figure 12, where f_w is plotted vs.

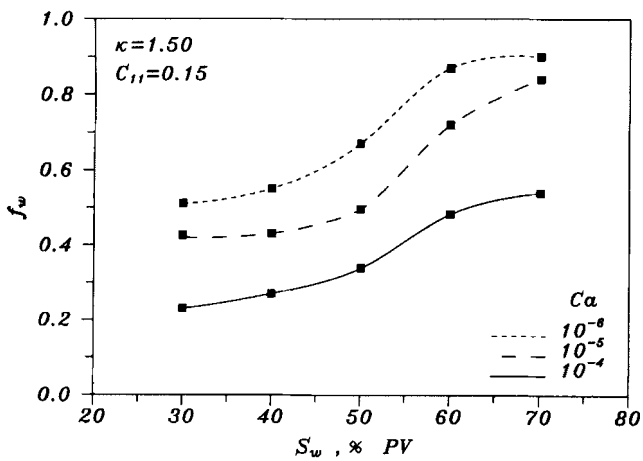

Figure 11. Fractional flow curves, $f_w(S_w)$, for three typical values of the capillary number ($Ca = 10^{-6}$, 10^{-5}, and 10^{-4}) and $\kappa = 1.50$, $C_{11} = 0.15$, $\theta_a^0 = 45°$, and $\theta_r^0 = 35°$.

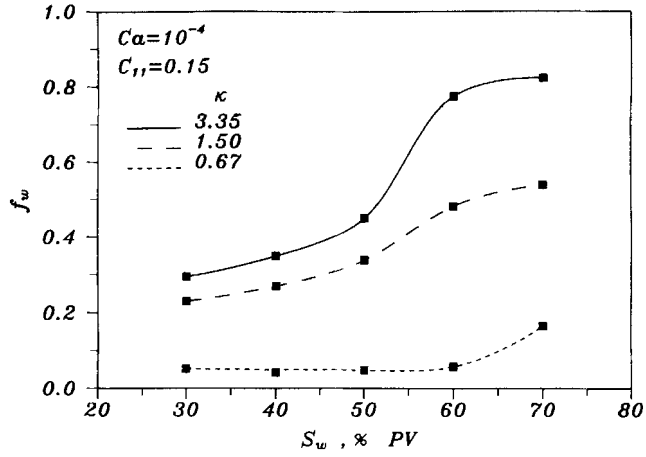

Figure 12. Fractional flow, $f_w(S_w)$, for three typical values of the viscosity ratio ($\kappa = 0.67$, 1.50, and 3.35) and $Ca = 10^{-4}$, $C_{11} = 0.15$, $\theta_a^0 = 45°$, and $\theta_r^0 = 35°$.

S_w for $\kappa = 0.67$, 1.50, and 3.35 and for $Ca = 10^{-4}$, $C_{11} = 0.15$, $\theta_a^0 = 45°$, and $\theta_r^0 = 35°$. This behavior has been verified also experimentally (Craig, 1971; Avraam and Payatakes, 1995). Figure 13 shows the dependence of f_w on C_{11} for various values of S_w and $\kappa = 1.50$, $Ca = 10\_5$, $\theta_a^0 = 45°$, and $\theta_r^0 = 35°$. These results confirm that f_w increases as s increases.

Relative permeabilities

The "steady-state" relative permeabilities values, k_{rw} and k_{ro}, are complex functions of several parameters,

$$k_{ro} = k_{ro}(S_o, Ca, \kappa, \cos\theta_a^0, \cos\theta_r^0, Co; \underline{x}, \text{saturation history}) \quad (4)$$

$$k_{rw} = k_{rw}(S_w, Ca, \kappa, \cos\theta_a^0, \cos\theta_r^0, Co; \underline{x}, \text{saturation history}) \quad (5)$$

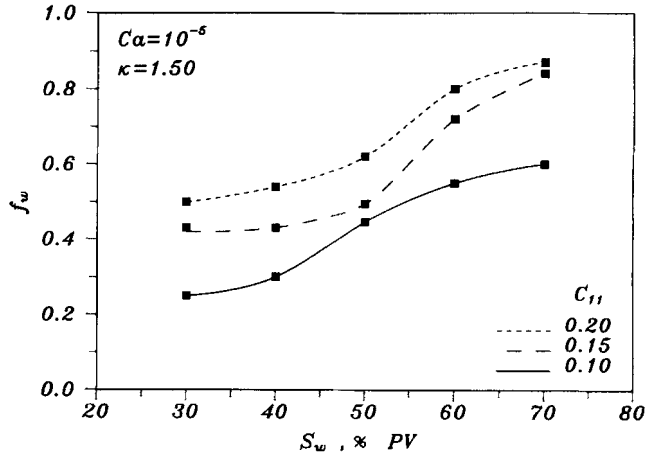

Figure 13. Fractional flow, $f_w(S_w)$, for three typical values of the probability of coalescence between two colliding ganglia ($C_{11} = 0.10$, 0.15, and 0.20) and $\kappa = 1.50$, $Ca = 10^{-5}$, $\theta_a^0 = 45°$, and $\theta_r^0 = 35°$.

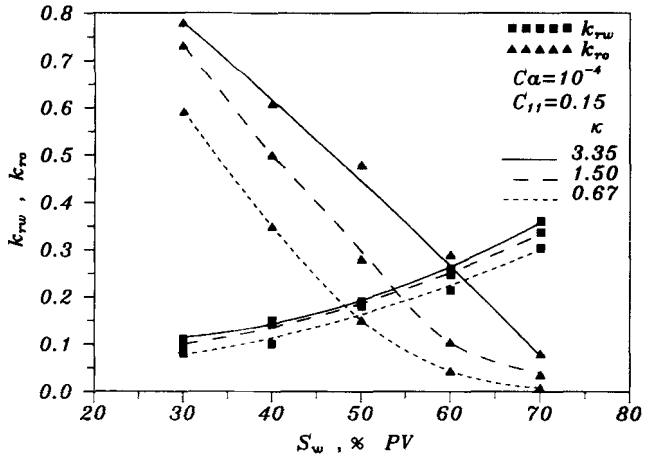

Figure 14. Dependence of the "steady-state" relative permeabilities to both fluids, k_{rw} and k_{ro}, on water saturation, S_w.

For typical values of the viscosity ratio ($\kappa = 0.67$, 1.50, and 3.35) and $Ca = 10^{-4}$, $C_{11} = 0.15$, $\theta_a^0 = 45°$, and $\theta_r^0 = 35°$.

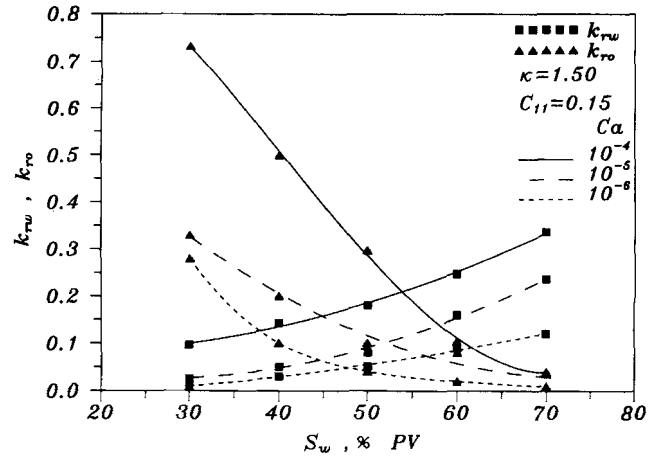

Figure 15. Dependence of the "steady-state" relative permeabilities to both fluids, k_{rw} and k_{ro}, on water saturation, S_w.

For three typical values of the capillary number ($Ca = 10^{-6}$, 10^{-5}, and 10^{-4}) and $\kappa = 1.50$, $C_{11} = 0.15$, $\theta_a^0 = 45°$, and $\theta_r^0 = 35°$.

This dependence is caused, among other things, by the way in which the oil is distributed in ganglia, the positions that the stranded ganglia occupy within the pore network, the paths that the moving ganglia follow, and other details pertinent to their motion. Consequently, k_{ro} and k_{rw} depend—among other things—on the "steady-state" mean ganglion size, $\langle v^* \rangle$, and the fraction of oil in the form of stranded ganglia, s. The flow phenomena taking place at pore level can be used to explain the behavior of k_{rw} and k_{ro}.

Figure 14 shows the dependence of k_{rw} and k_{ro} on the viscosity ratio, κ, and the water saturation, S_w, for $Ca = 10^{-4}$ and $C_{11} = 0.15$, $\theta_a^0 = 45°$, and $\theta_r^0 = 35°$. We observe that both k_{rw} and k_{ro} increase as κ increases. At this Ca value viscous effects are important and as κ increases, the oil (becoming more viscous) shows an increased tendency to select flow paths composed of large pores. Therefore, at medium and high Ca values as κ increases the two fluids tend to become more segregated, each one favoring certain pathways that permit a lower overall rate of viscous dissipation. This segregation causes the increase of both relative permeabilities. The experimental results of Lefebvre du Prey (1973) and Fulcher et al. (1985) show that the viscosity ratio increases the relative permeability to oil increases, whereas the relative permeability to water decreases. Note, however, that the aforementioned experimental data were obtained by changing both the fluid systems and the porous medium (core sample) simultaneously. Hence, the contact angles, which were not measured, could change and affect values of relative permeabilities significantly. Our theoretical predictions agree with experimental results of Avraam and Payatakes (1995), in which the contact angle was kept virtually constant.

For any fixed S_w value, both k_{rw} and k_{ro} increase as the capillary number, Ca, increases (Figure 15). This happens because as Ca increases, the portion of oil in the form of stranded ganglia, s, decreases (Figure 8), that is, the number of blocked pores decreases. This is in agreement with experimental results (Sandberg et al., 1958; Lefebvre du Prey, 1973; Amaefule and Handy, 1982; Fulcher et al., 1985; Avraam et al., 1994; Avraam and Payatakes, 1995).

Figures 16 and 17 show the dependence of k_{rw} and k_{ro} on S_w, Ca, and κ, for $C_{11} = 0.15$, $\theta_a^0 = 45°$, and $\theta_r^0 = 35°$. Figure 16 shows that k_{rw} is an increasing function of S_w, Ca, and κ (keeping all the other parameters constant), whereas Figure 17 shows that k_{ro} is an increasing function of $S_o (= 1 - S_w)$, Ca, and κ. Comparing the histograms of $\langle v^* \rangle$ (Figure 7) and k_{ro} (Figure 17) we observe that for relatively high $\langle v^* \rangle$ values, k_{ro} remains relatively small, whereas for relatively small $\langle v^* \rangle$ values k_{ro} is relatively high. These observations are also in qualitative agreement with the experimental results of Avraam and Payatakes (1995).

When the value of C_{11} increases, both the "steady-state" reduced mean ganglion volume, $\langle v^* \rangle$, and the fraction of oil in the form of stranded ganglia, s, increase (Figure 10). Thus, the number of blocked pores of the pore network increases as C_{11} increases. This is the reason for which both k_{rw} and k_{ro} decrease as C_{11} increases (Figure 18), keeping the other parameters constant ($Ca = 10^{-5}$, $\kappa = 1.50$, $\theta_a^0 = 45°$, $\theta_r^0 = 35°$). This behavior conforms with the observation that was made earlier, namely that k_{ro} is relatively small for relatively large $\langle v^* \rangle$ values, and large for small $\langle v^* \rangle$ values.

Case Study

In order to check the validity of the simulator, we are going to compare reported experimental results with the respective theoretical predictions. For this case, we chose to use experimental results of Avraam and Payatakes (1995) for the following two reasons: (1) The "steady-state" two-phase flow experiments were performed in a transparent planar porous medium, which permits the optical observation of the flow regime. Hence, we can choose experimental data in the flow regime of small or large ganglion dynamics, where the simulator is applicable. (2) The porous medium used in these experiments is a planar pore network of chamber-and-throat type etched in glass, which presents many similarities with the pore network used by the simulator. Specifically, we chose to model the case of "steady-state" two-phase flow of *n*-dodecane dyed with Sudan Red (nonwetting phase) and

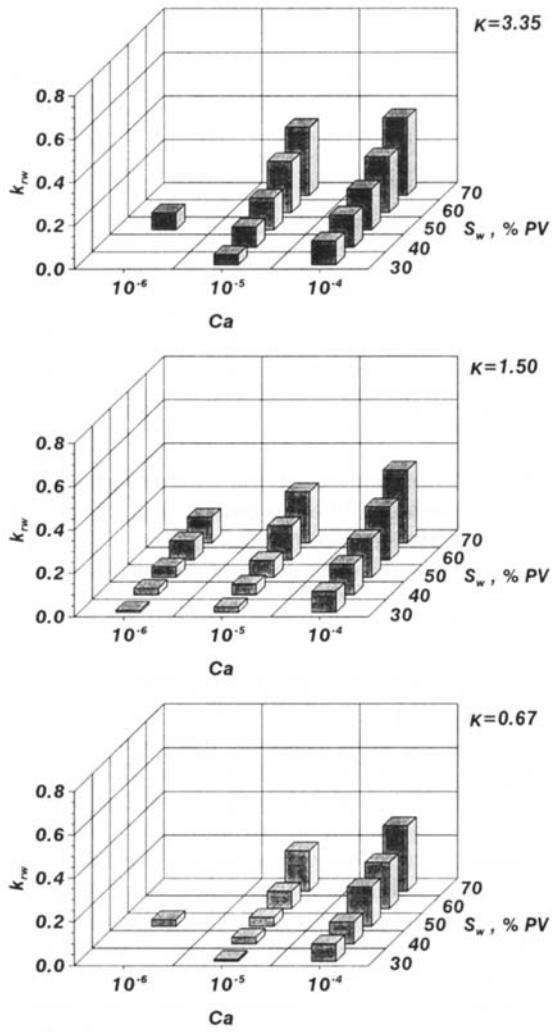

Figure 16. Map of the "steady-state" relative permeabilities to water, k_{rw}, as a function of the capillary number, Ca, water saturation, S_w, and the viscosity ratio, κ, for $C_{11}=0.15$, $\theta_a^0=45°$, and $\theta_r^0=35°$.

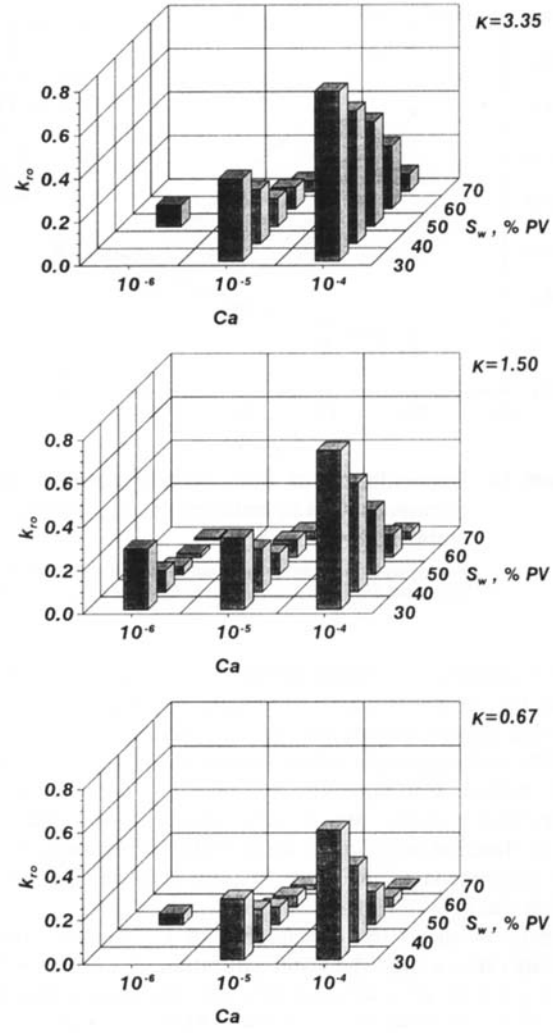

Figure 17. Map of the "steady-state" relative permeabilities to oil, k_{ro}, as a function of the capillary number, Ca, water saturation, S_w, and the viscosity ratio, κ, for $C_{11}=0.15$, $\theta_a^0=45°$, and $\theta_r^0=35°$.

deionized water (wetting phase). The viscosity ratio of this fluid system is $\kappa = 1.45$ and the equilibrium contact angle against glass is $\theta = 40°$ (Avraam and Payatakes, 1995). The value of the capillary number selected is $Ca = 1.2\times10^{-6}$ and the water saturation is in the range of $40\% \le S_w \le 65\%$ PV. Under these conditions the experimentally observed flow regime is ganglion dynamics (large ganglion dynamics for $S_w > 50\%$ and small ganglion dynamics for $S_w < 50\%$). The cross-sectional area of the pores of the porous medium used in the experiments has the shape of a biconvex lens, Figure 19b (Tsakiroglou and Payatakes, 1988; Vizika and Payatakes, 1989). These pores have a nearly constant (maximum) depth $w = 140$ μm, whereas the chamber widths are 280, 420, 560, 700 and 840 μm, and the throat widths are 56, 84, 112, 140 and 168 μm. Chamber and throat width distributions are discretized normal distributions, and the sizes of contiguous pores are uncorrelated. In the calculations we assume that each cross section of a pore is occupied by only one liquid. The exact solution of the flow field through a pore of biconvex lens shape is cumbersome. Given that such a solution must be repeated thousands of times during each simulation, we opted to use an analytical approximate solution, instead. The cross-sectional area is characterized by three diameters, namely, the equivalent capillary diameter, the equivalent area diameter, and the equivalent hydraulic diameter. All these diameters are functions of the pore aspect ratio, λ, that is, the ratio of the pore width, D, to the pore depth, w, given as $\lambda = D/w$. Tsakiroglou and Payatakes (1988) followed the approximate method of Mayer and Stowe (1965), also applied by Legait (1983) and Ransohoff et al. (1987), and obtained the equivalent capillary diameter of the biconvex lens area as

$$\frac{D_{cap}}{w} = \frac{(\lambda^2+1)\tan^{-1}\left(\dfrac{2\lambda}{\lambda^2-1}\right) - 2(\lambda^2-1)}{2(\lambda^2+1)\tan^{-1}\left(\dfrac{2\lambda}{\lambda^2-1}\right)}. \qquad (6)$$

This equivalent capillary diameter is used for the calculation of the pressure drop across the interfaces.

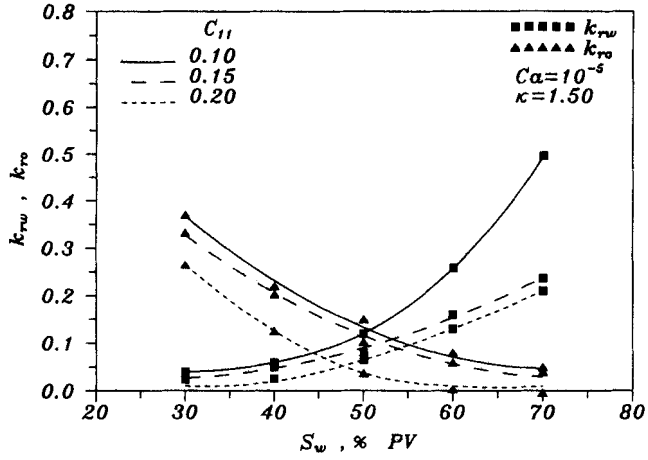

Figure 18. Dependence of the "steady-state" relative permeabilities to both fluids, k_{rw} and k_{ro}, on water saturation, S_w.

For three typical values of the probability of coalescence between two colliding ganglia ($C_{11} = 0.10$, 0.15, and 0.20) and $\kappa = 1.50$, $Ca = 10^{-5}$, $\theta_a^0 = 45°$, and $\theta_r^0 = 35.°$

The area of the biconvex lens cross section is equal to the area of two segments of a cycle of radius equal to $(D^2 + w^2)/4w$ (Tsakiroglou and Payatakes, 1988), and the equivalent area diameter is given by the expression

$$\frac{D_{\text{area}}}{w} = \left\{ \frac{1}{4\pi}(\lambda^2+1)^2 \left[\tan^{-1}\left(\frac{4\lambda(\lambda^2-1)}{(\lambda^2-1)^2 - 4\lambda^2} \right) - \frac{4\lambda(\lambda^2-1)}{(\lambda^2+1)^2} \right] \right\}^{1/2} . \quad (7)$$

Special care is taken in using Eqs. 6 and 7 to calculate angles in the appropriate quadrant from the inverse trigonometric functions. For simplicity we assume that the equivalent hydraulic diameter is equal to the equivalent area diameter. If the cross-sectional area of the pore were approximated as an ellipse, then its hydraulic diameter would differ less than 25% from the value calculated using Eq. 7, for the range of λ values used.

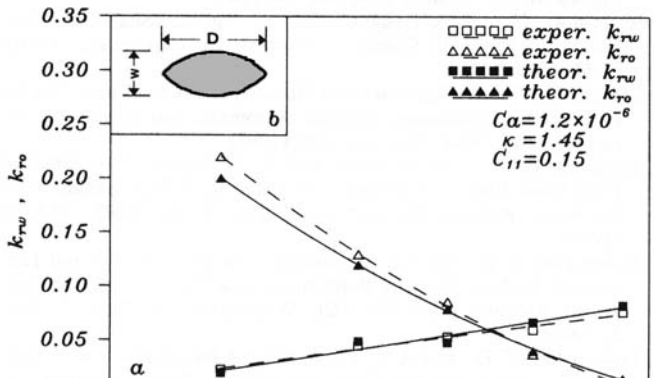

Figure 19. (a) Theoretical predictions of relative permeabilities vs. experimental data of Avraam and Payatakes (1995); (b) cross-sectional area of the pores of the model porous medium used in the experiments.

For $Ca = 1.2\times10^{-6}$, $\kappa = 1.45$, $\theta = 40°$, and $40\% \le S_o \le 65\%$ PV: for the theoretical results $C_{11} = 0.15$.

The dimensions of the planar pore network used in these simulations is $30\times30\times1$, and we set the value of the probability of coalescence between two colliding ganglia to $C_{11} = 0.15$. The relative permeabilities calculated by the simulator and the respective measured values from the experiments are shown in Figure 19a. The difference between these two sets of values ranges from 10 to 20%.

Conclusions

A computer-aided simulator of steady-state cocurrent two-phase flow through porous media in the flow regime of "steady-state" ganglion dynamics was developed. This simulator was used to study and analyze the flow behavior of the two fluids at pore level, to predict the (macroscopic) relative permeabilities, and to correlate the magnitude of the relative permeabilities with the flow mechanisms at pore level. The variables that were changed systematically are the water saturation (in the range $30 \le S_w \le 70\%$ PV), the capillary number (in the range $10^{-6} \le Ca \le 10^{-4}$), the viscosity ratio (in the range $0.67 \le \kappa \le 3.35$) and the effective probability of coalescence of a pair of colliding ganglia (in the range $0.10 \le C_{11} \le 0.20$), whereas the variables that were kept constant are the wettability (dynamic contact angles, $\theta_a^0 = 45°$ and $\theta_r^0 = 35°$) and the porous medium geometry and topology. The validity of the simulator was examined by comparing the theoretical predictions with the experimental results of Avraam and Payatakes (1995). Theoretical results are in good agreement with the aforementioned experimental results for the values of the parameters examined. The main conclusions that can be drawn from this study are the following:

- At "steady state" the oil is disconnected in the form of multisized ganglia, for the parameter values used. The motion of the oil occurs exclusively through the motion of ganglia. The motion and complex interactions of the ganglia can be denoted as *"steady-state" ganglion dynamics*.
- Ganglia show an increasing tendency to move through large pores as the viscosity ratio, κ, and/or the capillary number, Ca, decreases.
- The "steady-state" fractional flow of water, f_w, is an increasing function of the water saturation, S_w, the viscosity ratio, κ, the coalescence factor, Co, and a decreasing function of the capillary number, Ca, keeping the other parameters constant. The fractional flow of water, f_w, increases as s increases.
- The "steady-state" relative permeability to water, k_{rw}, is an increasing function of the water saturation, S_w, whereas the "steady-state" relative permeability to oil, k_{rw}, is an increasing function the oil saturation, S_o. Both k_{rw} and k_{rw} are increasing functions of the viscosity ratio, κ, and the capillary number, Ca, and decreasing functions of the coalescence factor, Co, keeping the other parameters constant. The relative permeability to oil, k_{ro}, increases as $\langle v^* \rangle$ decreases.
- The results of the present work provide valuable insights as to how the macroscopic behavior of "steady-state" two-phase flow in porous media depends on the pore-level flow mechanisms, and provide a means for understanding the effects of the numerous parameters that affect the flow.

Acknowledgments

This work was supported by Shell Research BV, KONINKLIJKE/SHELL—Exploratie en Produktie Laboratorium (KSEPL) and by the Institute of Chemical Engineering and High Temperature Chemical Processes. We thank Dr. Ilia Mitov (Univ. of Sofia, Bulgaria) for his assistance in developing better graphics (Figures 2 and 3).

Notation

D_{area} = equivalent area diameter of a pore of the biconvex lens shape (Eq. 7)
D_{cap} = equivalent capillary diameter of a pore of the biconvex lens shape (Eq. 6)
g = acceleration of gravity
L = distance along which the pressure drop is calculated ($L = 10\ l$)
q_o = flow rate of oil
q_w = flow rate of water
x = Cartesian coordinate, direction of macroscopic flow
y = Cartesian coordinate
z = Cartesian coordinate
μ_o = viscosity of oil

Literature Cited

Amaefule, J. O., and L. L. Handy, "The Effects of Interfacial Tensions on Relative Oil/Water Permeabilities of Consolidated Porous Media," *Soc. Pet. Eng. J.*, 371 (June, 1982).

Avraam, D. G., G. B. Kolonis, T. C. Roumeliotis, G. N. Constantinides, and A. C. Payatakes, "Steady-State Two-Phase Flow through Planar and Non-Planar Model Porous Media," *Transp. Porous Media*, **16**, 75 (1994).

Avraam, D. G., and A. C. Payatakes, "Flow Regimes and Mechanisms of Steady-State Two-Phase Flow in Porous Media," *J. Fluid Mech.*, **293**, 207 (1995).

Blunt, M., and P. King, "Relative Permeabilities from Two- and Three-Dimensional Pore Scale Network Modelling," *Transp. Porous Media*, **6**, 407 (1991).

Bryant, S., and M. Blunt, "Prediction of Relative Permeability in Simple Porous Media," *Phys. Rev. A*, **46**, 2004 (1992).

Constantinides, G. N., and A. C. Payatakes, "A Theoretical Model of Collision and Coalescence of Ganglia in Porous Media," *J. Colloid Interface Sci.*, **141**, 486 (1991).

Constantinides, G. N., and A. C. Payatakes, "A Three Dimensional Network Model for Consolidated Porous Media. Basic Studies," *Chem. Eng. Comm.*, **81**, 55 (1989).

Constantinides, G. N., and A. C. Payatakes, "Three-Dimensional Simulation of Immiscible Displacement of Oil Ganglia in Consolidated Porous Media," *Proc. Euro. Symp. Enhanced Oil Recovery*, Hamburg, F.R. Germany, p. 965 (1988).

Craig, F. F., *The Reservoir Engineering Aspects of Waterflooding*, Society of Petroleum Engineers of AIME, New York (1971).

Dias, M. M., and A. C. Payatakes, "Network Models for Two-Phase Flow in Porous Media: 1. Immiscible Microdisplacement of Non-Wetting Fluids," *J. Fluid Mech.*, **164**, 305 (1986a).

Dias, M. M., and A. C. Payatakes, "Network Models for Two-Phase Flow in Porous Media: 2 Motion of Oil Ganglia," *J. Fluid Mech.*, **164**, 337 (1986b).

Dullien, F. A. L., and G. K. Dhawan, "Bivariate Pore-Size Distribution of Some Sandstones," *J. Colloid Interf. Sci.*, **52**, 129 (1975).

Fulcher, R. A., T. Ertekin, and C. D. Stahl, "Effect of Capillary Number and Its Constituents on Two-Phase Relative Permeability Curves," *J. Pet. Tech.*, 249 (Feb., 1985).

Geffen, T. M., W. W. Owens, D. R. Parrish, and R. A. Morse, "Experimental Investigation of Factors Affecting Laboratory Relative Permeability Measurements," *Pet. Trans. AIME*, **192**, 99 (1951).

Goode, P. A., and T. S. Ramakrishnan, "Momentum Transfer Across Fluid-Fluid Interfaces in Porous Media: a Network Model," *AIChE J.*, **39**, 1124 (1993).

Hinkley, R. E., M. M. Dias, and A. C. Payatakes, "On the Motion of Oil Ganglia in Porous Media," *PhysicoChemical Hydrody.*, **8**, 185 (1987).

Honarpour, M., and S. M. Mahmood, "Relative-Permeability Measurements: An Overview," *J. Pet. Tech.*, 963, Aug. (1988).

Ivanov, I. V., and D. S. Dimitrov, "Thin Film Drainage," *Thin Liquid Films*, I. V. Ivanov, ed., Marcel Dekker, New York, p. 379 (1988).

Kantzas, A., and I. Chatzis, "Application of the Preconditioned Conjugate Gradients Method in the Simulation of Relative Permeability Properties of Porous Media," *Chem. Eng. Commun.*, **69**, 169 (1988a).

Kantzas, A., and I. Chatzis, "Network Simulation of Relative Permeability Curves Using a Bond Correlated-Site Percolation Model of Pore Structure," *Chem. Eng. Comm.*, **69**, 191 (1988b).

Koplik, J., and T. J. Lasseter, "Two-Phase Flow in Random Network Models of Porous Media," *SPE 11014, 57th Annual Fall Tech. Conf. and Exhibit of SPE*, New Orleans, LA, p. 26 (Sept., 1982).

Lefebvre du Prey, E. J., "Factors Affecting Liquid-Liquid Relative Permeabilities of a Consolidated Porous Medium," *Soc. Pet. Eng. J.*, 39 (Feb., 1973).

Legait, B., "Laminar Flow of Two Phases through a Capillary Tube with Variable Square Cross-Section," *J. Colloid Interface Sci.*, **96**, 28 (1983).

Lenormand, R., E. Touboul, and C. Zarcone, "Numerical Models and Experiments on Immiscible Displacements in Porous Media," *J. Fluid Mech.*, **189**, 165 (1988).

Li, Y., and N. C. Wardlaw, "The Influence of Wettability and Critical Pore-Throat Size Ratio on Snap-off," *J. Colloid Interface Sci.*, **109**, 461 (1986).

Mason, G., "Mobilisation of Oil Blobs in the Pore Space of a Random Sphere Packing," *Chem. Eng. Sci.*, **38**, 1455 (1983).

Mayer, R. P., and R. A. Stowe, "Mercury Porosimetry—Breakthrough Pressure for Penetration between Spheres," *J. Colloid Sci.*, **20**, 893 (1965).

McCaffery, F. G., and D. W. Bennion, "The Effect of Wettability on Two-Phase Relative Permeabilities," *J. Can. Pet. Tech.*, 42 (Oct.–Dec., 1974).

Ng, K. M., and A. C. Payatakes, "Stochastic Simulation of the Motion, Breakup and Stranding of Oil Ganglia in Water-Wet Granular Porous Media during Immiscible Displacement," *AIChE J.*, **26**, 419 (1980).

Owens, W. W., and D. L. Archer, "The Effect of Rock Wettability on Oil-Water Relative Permeability Relationships," *J. Pet. Tech.*, 873 (July, 1971).

Payatakes, A. C., "Dynamics of Oil Ganglia During Immiscible Displacement in Water-Wet Porous Media," *Ann. Rev. Fluid Mech.*, **14**, 365 (1982).

Payatakes, A. C., and M. M. Dias, "Immiscible Microdisplacement and Ganglion Dynamics in Porous Media," *Rev. Chem. Eng.*, **2**, 85 (1984).

Ramakrishnan, T. S., and D. T. Wasan, "Effect of Capillary Number on the Relative Permeability Function for Two-Phase Flow in Porous Media," *Powder Tech.*, **48**, 99 (1986).

Ransohoff, T. C., P. A. Gauglitz, and C. J. Radke, "Snap-Off of Gas Bubbles in Smoothly Constricted Noncircular Capillaries," *AIChE J.*, **33**, 753 (1987).

Sahimi, M., "Flow Phenomena in Rocks: From Continuum Models to Fractals, Percolation, Cellular Automata, and Simulated Annealing," *Rev. Mod. Phys.*, **65**, 1393 (1993).

Sandberg, C. R., L. S. Gournay, and R. F. Sippel, "The Effect of Fluid-Flow Rate and Viscosity on Laboratory Determinations of Oil-Water Relative Permeabilities," *Petr. Trans. AIME*, **213**, 36 (1958).

Tsakiroglou, C. D., and A. C. Payatakes, "An Experimental and Theoretical Study of Mercury Porosimetry in a Pore Network Model," AIChE Meeting, paper No. 102L, Washington, DC (Nov. 27–Dec. 2, 1988).

Tsakiroglou, C. D., and A. C. Payatakes, "A New Simulator of Mercury Porosimetry for the Characterization of Porous Materials," *J. Colloid Interf. Sci.*, **137**, 315 (1990).

Tsakiroglou, C. D., and A. C. Payatakes, "Effects of Pore-Size Correlations on Mercury Porosimetry Curves," *J. Colloid Interf. Sci.*, **146**, 479 (1991).

Vizika, O., D. G. Avraam, and A. C. Payatakes, "On the Role of the Viscosity Ratio During Low Capillary Number Forced Imbibition in Porous Media," *J. Colloid Interf. Sci.*, **165**, 386 (1994).

Vizika, O., and A. C. Payatakes, "Parametric Experimental Study of Forced Imbibition in Porous Media," *PhysicoChem. Hydrody.*, **11**, 187 (1989).

Manuscript received June 21, 1994, and revision received Mar. 1, 1995.